express
polymer letters

Research article

On isotactic polypropylene annealing: Difference in final properties of neat and β-nucleated polypropylene

Lenka Gajzlerova[1] , *Jana Navratilova*[1]* , *Sona Zenzingerova*[1] , *David Jaska*[1] ,
Lubomir Benicek[1] , *Michal Kudlacek*[1] , *Roman Cermak*[1] , *Martin Obadal*[2]

[1]Department of Polymer Engineering, Faculty of Technology, Tomas Bata University in Zlin, Vavreckova 275,
 760 01 Zlin, Czech Republic
[2]Borealis Polyolefine GmbH, St. Peter Strasse 25, 4021 Linz, Austria

Abstract. The effect of isotactic polypropylene (iPP) molecular weight and thermal treatment on final crystalline structure and mechanical properties were investigated by X-ray scattering, differential scanning calorimetry, tensile testing, and scanning electron microscopy. Neat and β-nucleated isotactic polypropylene were subjected to annealing above melting temperature of β-phase but still below melting temperature of α-phase, which caused both improvement of α crystallites and β to α-recrystallization, in case of nucleated material. As a consequence, the final mechanical properties like tensile strength and stiffness improved significantly. The increase is much more pronounced in the case of β to α-transformed materials with lower molecular weight. This phenomenon can also be attributed to the partial preservation of the specific structure of the amorphous phase present in β-nucleated polypropylene, in addition to the perfection of the crystalline phase. The amorphous phase comprises many interconnecting chains passing through several lamellae whereby providing a long-range effect.

Keywords: *mechanical properties, isotactic polypropylene, annealing, crystallinity, polymorphism*

1. Introduction

Isotactic polypropylene (iPP) is an important commodity plastic not only for its favorable price-performance ratio but also in view of its crystallographic modifications in which it can occur. The material has been attracting attention for decades since the revelation of particular structures. As a semicrystalline polymer, iPP crystallizes in monoclinic α-phase, trigonal β-phase (formerly referred to as hexagonal) [1–5], orthorhombic γ-phase, and so-called smectic form, which consists of rather small irregular crystallites [4–9]. During the crystallization from the molten state, essentially the α-phase is formed, accompanied by the amount of β crystallites [10]. It is well known that the end-use properties are closely connected with the supermolecular structure of polymorphic polymers. By controlling the supermolecular structure,

the properties of polymorphic materials can be tailored. The stiffness and strength are commonly related to the α-phase, while the β-phase is characterized by toughness and drawability, which is, unfortunately, accompanied by lower thermal stability.

Specific nucleation by addition of β-nucleating agent (NA) is an efficient way of achieving a certain amount of β-phase in the polymer [10–15]. The generally accepted view is that the microstructural changes are driven by annealing-induced secondary crystallization. Crystalline structure is exactly driven by various mechanisms as improvement of faulty crystals, thickening and lateral growth of primary lamellae, recrystallization, phase transformation, or a new arrangement of forced molecular chain in the amorphous phase. This leads to the limitation of defects and residual stresses in iPP [16–19].

---

*Corresponding author, e-mail: j1navratilova@utb.cz

In a common polypropylene spherulite, the annealing cannot significantly influence the supermolecular structure but only fine-tune the crystal structure within the spherulites [3, 20–23]. The β crystallites are metastable with the possibility of transformation into the more stable α-phase under heating conditions [13, 24]. By annealing at a temperature above melting temperature (T_m) for β-phase (≈155 °C) and under T_m for α-phase (≈170 °C), recrystallization of metastable β to α-phase can be achieved, as α crystals grow faster at high temperatures, above the critical temperature ($T^* \approx 141$ °C). Lotz [24] proposed that in standard iPP, both α→β and β→α recrystallization is possible at certain heating conditions. Since the temperature used in this paper is 160 °C, the nucleation effect of NA should be negated, and β→α recrystallization is assumed. Transformation of β crystallites to more thermally stable α crystallites gained interest in recent times, primarily in the scientific area. For example, Bai and coworkers [25, 26], and Na *et al.* [27] showed that annealing is an effective method to promote chain rearrangement. In all papers mentioned before, injection-molded specimens were used, and the transformation of highly oriented material into more thermodynamically stable conformation with consequent effects on final properties was studied. Unfortunately, none of them focused directly on β to α recrystallization. This process was partly studied by Kotek *et al.* [7]; however, the annealing temperature used in their paper was lower than the one used in the present paper; thus, the β crystallites were able to remain and to thicken during the thermal treatment.

The goal of the present study is to investigate the influence of iPP molecular weight and annealing on final mechanical properties. It is thought that annealing at high temperature, which destroys β crystallites but is still below a melting temperature of α crystallites, enables the formation of enhanced thicker lamellae and some improvement of final mechanical properties.

2. Experimental section
2.1. Materials
Commercial-grade isotactic polypropylenes *BE52* and *HD601CF*, both produced by Borealis Polyolefine GmbH, Austria, were used in the present study. The former material is characterized by a melt flow index (MFI) of 0.25 g/10 min, weight-averaged molecular weight (M_w) of 1 300 000, and polydispersity

index (PDI) 4.0, while the latter has MFI of 8 g/10 min, M_w of 570 000 and PDI 3.5. Both MFIs are according to ISO 1133 (230 °C and 2.16 kg) as listed in relevant datasheets; the M_w and PDI values were measured using gel permeation chromatography (GPC). Specific β-nucleating agent *N,N′*-dicyclohexylnaphthalene-2,6-dicarboxamide in powder form was produced by Rika Int., Manchester, Great Britain. Materials were premixed with 0.3 wt% of paraffinic oil to ensure sufficient NA dispersion and then mixed with 0.03 wt% NA and without NA using Brabender twin-screw extruder [28, 29]. The processing conditions were as follows: screw speed 50 rpm; temperatures of barrel zones 190, 200, and 220 °C. Both materials – neat and nucleated were used in the study. Standard dumbbell specimens with gauge length 50 mm, width 10 mm, and thickness 4 mm (ISO 527-2/1A) were injection-molded with DEMAG Ergotech 50-200 System injection-molding machine. The processing conditions are summarized in Table 1.

Nomenclature of materials in this paper follows this pattern: the material is denoted in first four characters – BE52 and HD60 for BE52 and HD601CF, respectively. These are followed by suffix '-nu' in case of β-nucleated materials or '-an' for samples which underwent thermal treatment.

2.2. Annealing
Specimens were kept at room temperature (25 °C) for 24 h after their production. One half of specimens of each material were then stored in a refrigerator (5 °C) to suppress further structural changes. The other half was exposed to annealing by air in an oven. The annealing temperature was 160 °C, and the exposure time was 60 min, after which the heating was turned off while the specimens were kept inside the oven to cool down for five hours. Annealed specimens were stored in a refrigerator before further use.

Table 1. Processing conditions of injection molding.

Feeding zone temperature	[°C]	50
Heating zone temperatures	[°C]	240–250–260
Die temperature	[°C]	260
Mold temperature	[°C]	60
Injection speed	[mm/s]	40
Injection pressure	[MPa]	75
Holding pressure	[MPa]	45
Holding pressure time	[s]	25
Freezing time	[s]	20

2.3. Differential scanning calorimetry

Investigation of thermal behavior was conducted by using a Mettler Toledo DSC 1 instrument. About 7–9 mg of each material was cut using a microtome. The cuts were taken perpendicularly to the test specimen axis to keep the same skin/core ratio as there might be a difference in phase composition. The material was closed in an aluminum pan and measured with an empty pan as a reference. All measurements were initiated by short settling at 25 °C (1 min). Subsequently, heating from 25 to 200 °C was done with a heating rate of 10 °C/min. At 200 °C, the samples were kept isothermally for 3 min. After that, they were cooled with the rate of –10 °C/min down to 25 °C. The heating/cooling cycle was repeated once again to obtain a melting peak that is not affected by preceding processing. All the measurements were performed under nitrogen as a purge constantly passing (20 ml/min) the DSC cell.

Values of each enthalpy change were gained using the instrument software. The heat of fusion (ΔH_m) was then recalculated using Equation (1) to estimate the crystallinity of annealed and untreated samples. The heat of fusion of fully crystallized iPP ($\Delta H_m^0 =$ 146 and 113 J/g for α and β crystallites, respectively) was taken from the previous publication [30]:

$$x_c = \frac{\Delta H_m}{\Delta H_m^0} \cdot 100 \tag{1}$$

Gibbs-Thomson equation (Equation (2)) was employed to calculate lamellar thickness (l_c) of each sample using peak position (melting temperature, T_m). Material constants are listed in Table 2 [31, 32]:

$$T_m = T_m^0 \left(1 - \frac{2\sigma_e}{\Delta h_f l_c}\right) \tag{2}$$

2.4. Wide-angle X-ray scattering

To reveal the crystalline structure of the studied materials, a PANalytical X'Pert Pro X-ray diffractometer

Table 2. Constants are used to calculate the lamellar thickness [31, 32].

Name	α crystallites	β crystallites
Equilibrium melting temperature, T_m^0 [°C]	208	176
Volumetric enthalpy of fusion, Δh_f [J/m³]	1.96·10⁸	1.77·10⁸
Fold surface energy, σ_e [J/m³]	0.122	0.05

with Ni-filtered CuKα radiation (λ = 0.154 nm) was used. All the measurements were performed at 40 kV and 30 mA. The angle of incidence varied from 10 to 30° (2θ) by steps of 0.013°. Both skin and core were measured; the core was revealed by grinding off about 1 mm of the skin layer. Each spectrum was decomposed by using a Gaussian peak with a fixed maximum at 17° (amorphous halo) [33–35] and up to six individual peaks defined with Pearson VII function (reflections of the crystalline phase). The overall crystallinity (X_C) was then calculated with Equation (3) where A_c and A_a are the fitted areas of crystal and amorphous peaks, respectively [27]:

$$X_C = \frac{\sum A_c}{\sum A_c + \sum A_a} \tag{3}$$

The relative amount of the β crystals (K_β) was evaluated by the method of Turner Jones and coworkers [1, 36] represented by Equation (4) where A_{300}^β is the area of the (300) reflection peak, A_{110}^α, A_{040}^α, and A_{130}^α are the areas of the (110), (040), and (130) reflection peaks, respectively:

$$K_\beta = \frac{A_{300}^\beta}{A_{300}^\beta + A_{110}^\alpha + A_{040}^\alpha + A_{130}^\alpha} \tag{4}$$

The overall crystallinity can then be divided into the β crystals (X_β) and the α crystals (X_α) crystallinity according to Equations (5) and (6):

$$X_\beta = K_\beta \cdot X_C \tag{5}$$

$$X_\alpha = X_C - X_\beta \tag{6}$$

WAXS record can be further analyzed with Scherrer equation (Equation (7)), which gives the length L_{hkl} of crystallite domain in the direction perpendicular to (hkl):

$$L_{hkl} = \frac{K \cdot \lambda}{FWHM \cdot \cos 2\theta} \tag{7}$$

where λ stands for the wavelength of used X-ray, *FWHM* is the full width at half maximum of the relevant peak, while the 2θ is the peak position, both values are in radians. The constant K is referred to vary from 0.8 to 1.3 according to particle shape [33, 37], but in this paper, the constant was omitted by setting it to 1 as, for example, in Kotek *et al.* [38]. It is worth noting that the length L_{hkl} can also be expressed as Equation (8):

$$L_{hkl} = \bar{N} \cdot d_{hkl} \qquad (8)$$

where $\bar{N}$ is the mean number of parallel planes (*hkl*) separated by d_{hkl}. Although Equation (7) is sometimes used to estimate the size of the crystalline region, in the case of polymers, the numerical results are rather unreliable because of the prevalence of lattice distortions, which disturb parallelism of (*hkl*) planes [23]. These distortions then cause broadening of relevant reflection, which is not connected with the crystallite size but primarily with its perfection. The higher the L_{hkl} value, the smaller number of distortions, thus higher crystal perfection.

2.5. Tensile testing

Tensile properties of the specimens were tested at ambient temperature (25 °C) by means of a Zwick 1456 universal testing machine. Six specimens of each annealed and untreated set of each material were strained at the initial rate of 1 mm/min to 0.5% strain to accurate determination of Young's modulus. Subsequently, the testing continued at the strain rate of 100 mm/min.

2.6. Scanning electron microscopy

The surface intended for observation by means of scanning electron microscopy (SEM) was firstly smoothed by cutting with a microtome and subsequently chemically etched. 1 wt% solution of $KMnO_4$ in 86% H_2SO_4 was used for the etching at room temperature for 15 min. After washing in running water for 10 min, specimens were washed with acetone and sputter-coated with Pd/Au alloy. An FEI Quanta FEG scanning electron microscope (SEM) was used for the observation employing Everhart-Thornley detector, and 5 kV accelerated voltage.

3. Results and discussion

Figure 1 gives a comparison of the melting behavior of all samples during the first heating. One can clearly see that all curves of annealed samples have only one peak shifted to a higher temperature, while the untreated materials have expectable peaks according to the present phases. The sharpness and intensity of β-phase melting peaks are, however, poor, which may be related to the recrystallization effects, as showed by Yamamoto *et al.* [39]. The exact positions of each peak are summarized in Table 3 together with evaluated ΔH_m, l_c, and x_c. Crystallinity derived from the DSC measurement has a similar trend as in
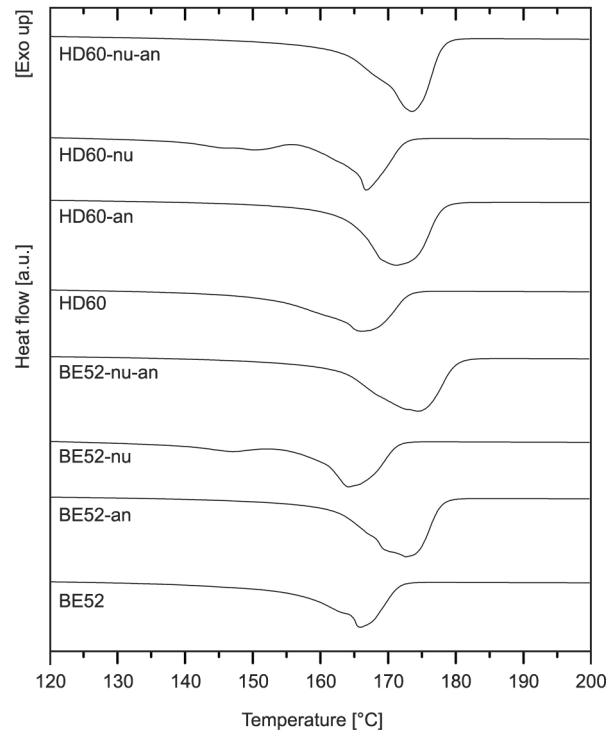

Figure 1. First heating run of annealed and untreated samples. Curves are mass-normalized and shifted vertically to better distinguish.

the case of values derived from X-ray spectra (cf. Table 4). The values, however, differ, and in the further text the crystallinity and phase composition established from the X-ray measurements is discussed as there is an assumption that these are more exact than values estimated from DSC, in which recrystallization usually occurs.

After complete melting of the material, samples were cooled down. Subsequently, a second heating run was performed to check whether any degradation or long-lasting changes happened during the annealing. This method is more suitable for observing

Table 3. Melting temperatures and characteristics established from DSC records.

		T_m [°C]	T_c [°C]	ΔH_m [J/g]	l_c [nm]	x_c [%]
BE52	α-phase	165.9	119.7	77.8	14.27	53
BE52-an	α-phase	172.6	119.0	106.1	16.99	73
BE52-nu	α-phase	164.2	125.3	66.4	13.72	46
	β-phase	147.1	–	24.7	9.18	22
BE52-nu-an	α-phase	174.4	124.5	109.1	17.90	75
HD60	α-phase	166.1	115.7	88.7	14.34	61
HD60-an	α-phase	171.2	116.3	113.5	16.34	78
HD60-nu	α-phase	166.7	124.9	59.1	14.55	41
	β-phase	150.4	–	25.8	10.37	23
HD60-nu-an	α-phase	173.6	125.0	113.7	17.48	78

the early stages of thermooxidative degradation than infrared spectroscopy [40]. Record of cooling revealed no significant information besides the effect
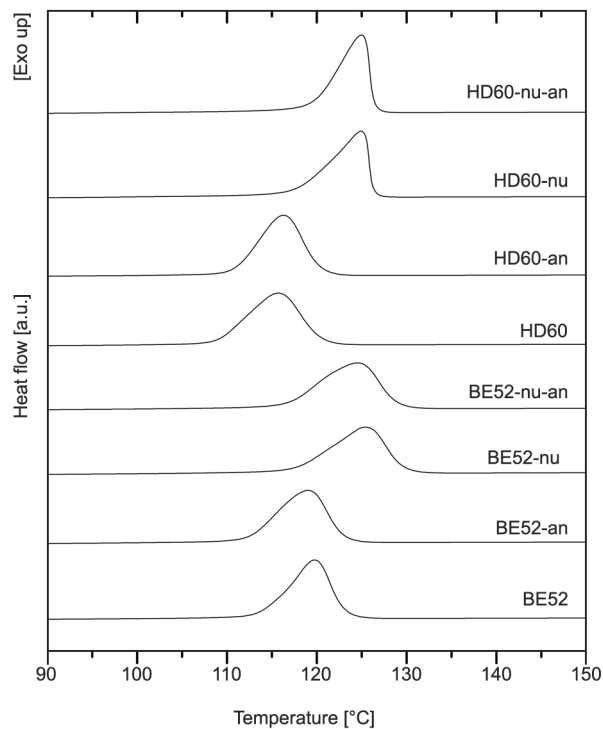

Figure 2. Cooling run of annealed and untreated samples. Curves are mass normalized and shifted vertically to better distinguish.
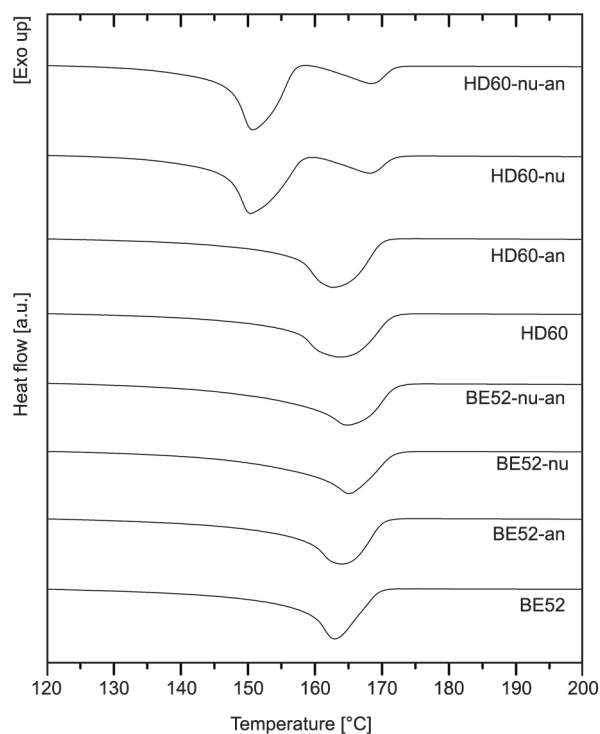

Figure 3. Second heating run of annealed and untreated samples. Curves are mass normalized and shifted vertically to better distinguish.

of nucleating agent, which was expected and can be seen in Figure 2. The record of the second melting is presented in Figure 3. By comparing the melting curve profiles of the second heating run before and after annealing, small differences in peaks are visible. This could be connected with thermooxidative degradation. Both HD60-nu and HD60-nu-an showed typical peaks observed in most cases of β-nucleated materials [28, 41, 42], while the high-molecular weight iPP, *i.e.*, BE52-nu and BE52-nu-an, exhibited only peak related to α-phase melting. This material was investigated further with DSC, and it was observed that:

(i) Crystallization peak is at higher temperatures than the non-nucleated equivalent indicating, the heterogeneous crystallization; thus, the effect of NA is proved.

(ii) Presence and intensity of the β-phase melting peak is related to the speed of cooling – no peaks were observed in case of slow cooling (–5, or –10 °C/min) while at cooling rate –20 °C/min the peak is manifested and it was more pronounced at higher cooling rates (–40 and –80 °C/min). This corresponds to the relation between β-phase creation and cooling rates studied by Varga and Menyhárd [42].

The β-nucleated materials which underwent annealing revealed no peak of β-phase; thus, the recrystallization of β-phase into a more stable α-phase happened during the treatment. Comparing these peaks with relevant peaks of non-nucleated materials (Figure 1), one can see that their maxima are at higher temperatures, which is even more pronounced in the case of HD60 and HD60-nu pair. After recalculation of lc (Table 3) it is clear that the lamellae thickened in the process – the highest increase was in the case of BE52-nu and BE52-nu-an pair (30%), while the lowest increase was in HD60 and HD60-an pair (14%). The increase of lamellar thickness within the other two pairs (pure BE52 and HD60-nu) was about 20%. BE52-related materials comprise of high molecular weight chains, which are more likely to entangle than the HD60-related materials. Moreover, the β-nucleation favors β crystals, which melt at the temperature used in annealing; thus, there was enough material from both melted β-phase and freed movable segments of bends and ties, which enabled perfection with the highest ratio. On the other hand, the HD60 and HD60-an pair, which molecular weight is half of the previous pair, has shorter chains. This enabled the

evolution of crystalline areas in a single step, and as there were no β crystals to melt, the increase in lamellar thickness by the perfection of the structure was limited. The disappearance of the β-phase after the annealing was confirmed by missing WAXS reflection of the (300) plane in relevant WAXS patterns.

Figure 4 presents X-ray diffraction patterns of all samples. Typical diffraction spectra of two-phase crystalline system with monoclinic α-phase – main planes of the α_1 (110), α_2 (040) and α_3 (130), and/or trigonal β-phase (300) can be seen. Untreated iPP with lower
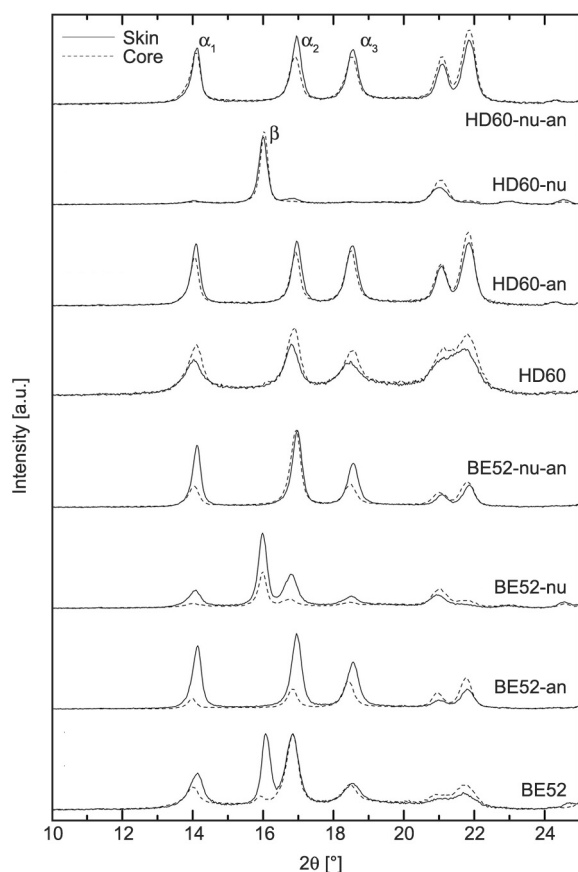
molecular weight (HD60) consists predominantly of monoclinic α-phase, while BE52 crystallizes into α-phase and moreover into β-phase, especially in the skin layer. The strong dependence of polymorphic composition on molecular weight in the case of nucleated iPP can be seen. While the addition of NA leads to the formation of almost solely trigonal β-phase in the case of HD60-nu (lower M_w), the co-existence of α- and β-phase in BE52-nu (higher M_w) is evident. This phenomenon can be explained by the notion of competition between self-nucleation and heterogeneous β-nucleation. The number of self-nuclei should be lower in low molecular weight iPP [28]. On the other hand, annealing practically negates the nucleation activity of the β-nucleating agent, the content of the β-phase is virtually zero in all samples, and they crystallize exclusively into the monoclinic α-phase.

Concerning the calculated values (Table 4) of the lamellae length in (110) and (300) direction of the α and β crystallites, respectively, which correspond to the crystal growing planes [30], the increase of the L_{110} during annealing is evident. This information indicates that the α crystallites stopped their growth due to lower mobility of chains as the material cooled down and also due to the lack of crystallizable material, which was consumed by the fast growing β crystallites [32] and that their growth was restored during annealing. The increase in length can then be caused by two phenomena – secondary nucleation on the (110) face of crystallite – *i.e.*, continuation in the previously terminated growth; and crystallization of the interlamellar chains, which as a consequence led to joining of two or more crystallites into one longer. The highest increase in length is seen in the case of lamellae localized in the skin layer, which is probably caused by a lower degree of

Figure 4. X-ray diffraction patterns of all samples.

Table 4. Crystallinity and lamellar length calculated from WAXS data.

	Skin			Core			Skin				Core			
	K_β [–]	X_β [%]	X_α [%]	K_β [–]	X_β [%]	X_α [%]	L_{110} [nm]	L_{040} [nm]	L_{130} [nm]	L_{300} [nm]	L_{110} [nm]	L_{040} [nm]	L_{130} [nm]	L_{300} [nm]
BE52	0.25	19	57	0.06	5	72	17.7	20.2	13.8	29.2	19.4	21.4	16.1	16.5
BE52-an	–	–	73	–	–	79	28.6	25.8	21.5	–	25.6	19.3	21.0	–
BE52-nu	0.45	33	41	0.59	39	27	18.1	19.9	14.1	29.1	18.7	23.8	16.4	33.4
BE52-nu-an	–	–	87	–	–	77	30.1	25.8	24.0	–	23.8	26.0	26.0	–
HD60	–	–	66	–	–	75	16.6	19.3	12.7	–	17.2	20.5	14.4	–
HD60-an	–	–	77	–	–	80	28.8	25.9	21.6	–	28.8	28.0	23.7	–
HD60-nu	0.83	61	12	0.95	69	4	15.0	13.9	–[a]	27.8	13.8	19.0	12.8	33.0
HD60-nu-an	–	–	84	–	–	79	28.6	26.8	23.7	–	24.0	24.0	22.9	–

[a]Reflection (130) was not found during the decomposition of this spectrum.

orderliness since this layer is frozen first when it comes in contact with the cooled mold surface. During the annealing, the skin layer is also the first part of the specimen, which is heated up; thus, the skin has more time to rearrange its structure than the core part has. Regarding crystallinity values (Figures 5 and 6) established from the deconvolution of WAXS patterns, the crystallinity generally increased after the annealing. The highest increases are seen in both cases of nucleated iPP when measured through the skin layer, while the increase in the case of non-nucleated materials is lower. The difference before and after annealing is also smaller when measured in the core of specimens (Figure 6). This can be caused by the fact that the skin layer had frozen as first; thus, the material had less time to create an ordered structure, as

previously described. When annealed, the presence of amorphous material and melt of former β crystallites enabled perfection and growth in larger extension than it possibly happened in the core region.
Figures 7 and 8 show the dependence of tensile stress on elongation of the specimen, while Figures 9 to 11 give a summary of main properties – Young's modulus, maximal stress (stress at yield) the specimen can bear before significant plastic deformation become evident, and elongation at break.
Regarding the maximum tensile stress (Figure 9), the lowest value was measured in the case of HD60-nu before annealing, and the same material showed the highest value after the annealing. Related to each other, the character of deformation changed from ductile with the highest achievable elongation in the
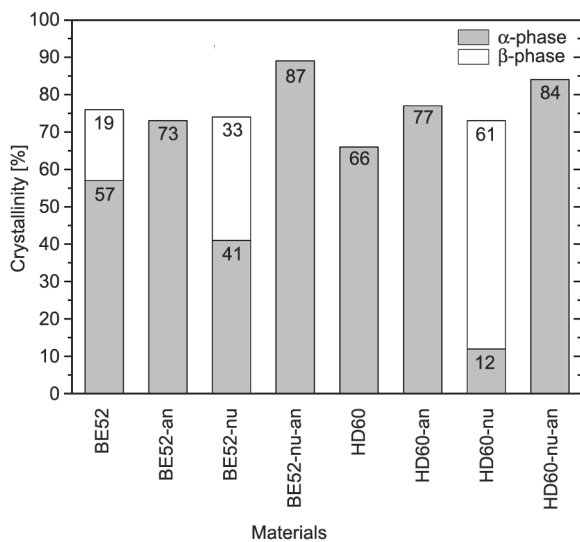

Figure 5. Comparison of crystallinity values calculated from the decomposition of WAXS spectra measured through the skin layer.
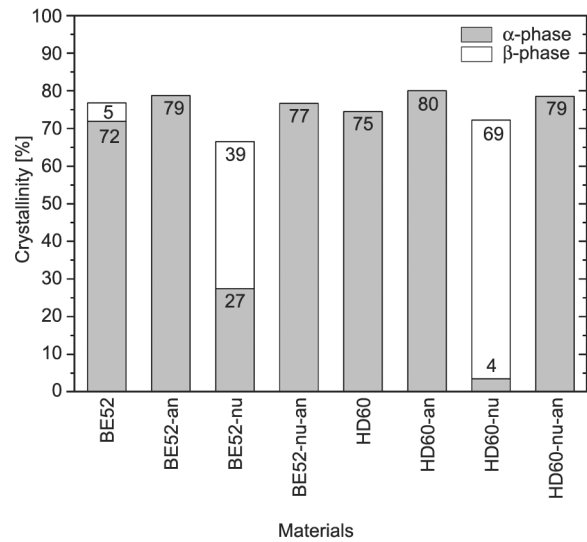

Figure 6. Comparison of crystallinity values calculated from the decomposition of WAXS spectra measured in the specimen core.
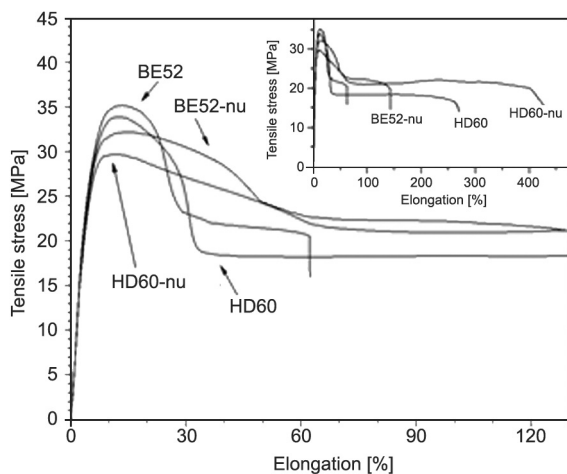

Figure 7. Record of tensile test – averaged curves, thermally untreated samples. Inset shows full x axis.
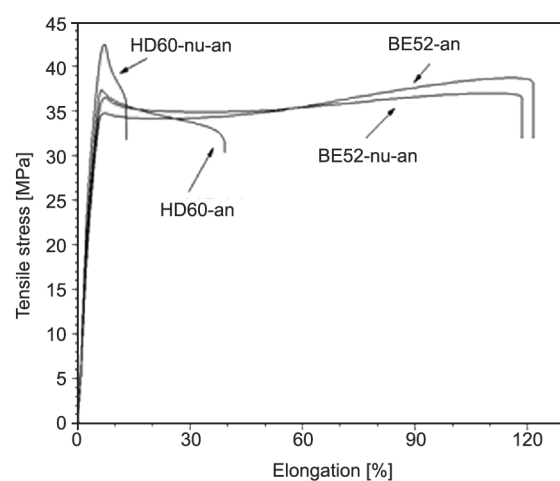

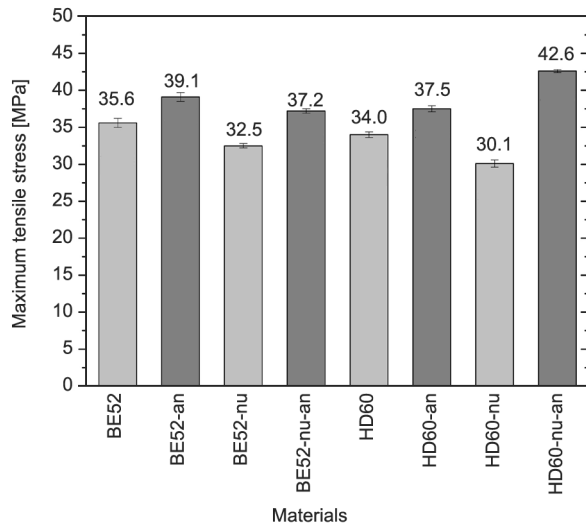**Figure 8.** Record of tensile test – averaged curves, annealed samples.

Figure 9. Comparison of maximum tensile stress; light bars are untreated specimens, and dark bars are specimens after annealing.
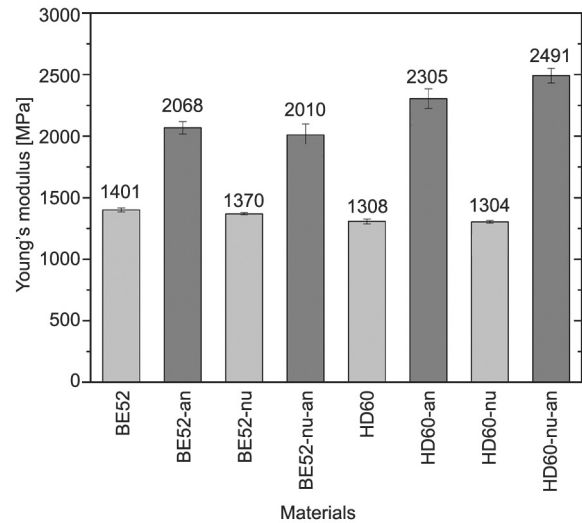

Figure 11. Comparison of Young's moduli; light bars are untreated specimens, and dark bars are specimens after annealing.
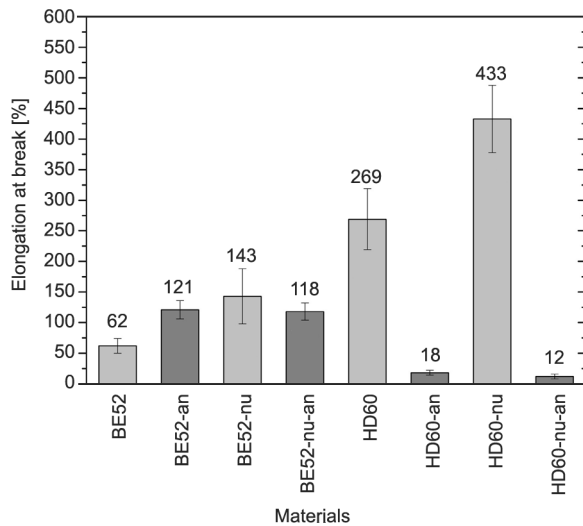

Figure 10. Comparison of maximal elongations achieved before specimens broke; light bars are untreated specimens, and dark bars are specimens after annealing.

set to the most brittle with negligible plastic deformation before the break (see Figure 10). This corresponds to the recrystallization of β- to α-phase. A similar trend was observed in the BE-52-nu pair before/after annealing, where the difference is not as strong. The maximum tensile stress in materials BE52 and HD60 also increases, while elongation at break for those materials is substantially different (Figure 10). In the case of high molecular weight BE52, elongation increased after annealing, while lower molecular weight HD60 showed a substantial decrease in elongation after annealing. The molecular weight evidently has an effect on mechanical behavior and will be discussed further in this study.

Comparing values of Young's modulus (Figure 11), the highest increase (over 90%) is seen again in the case of pair of HD60-nu before/after annealing, while a significant increase is also in the case of neat HD60 (76%). The increase in the case of BE52-related materials is lower; however, it reaches about 47% in the case of both neat and nucleated materials.

When comparing the information about supermolecular structure with the mechanical quality, it is evident that the materials which underwent annealing have virtually the same crystallite dimensions. Despite this fact, the mechanical properties differ when comparing neat and nucleated material after annealing. A significant increase is evident in the case of HD60 and HD60-nu, both after annealing. This indicates two facts:

 (i) Neither the crystallinity nor the crystallite size has a major impact on the strength or stiffness.
 (ii) Significant increase in both stiffness and strength, accompanied by a decrease in drawability, is achievable in the case of material with lower M_w.

Since the crystalline part of the materials is quite similar, the change in mechanical behavior may be driven by the amorphous phase.

In the case of iPP, the folded chain lamellae are typical for the α-phase. In this case, the major part of the chains is comprised of one lamella, and only a minor part of the chains is creating ties between two or more lamellae. It is also suggested that the β-phase crystallites are created by extended chains that pass through many lamellae and amorphous interlayers. The amorphous phase then contains a high amount
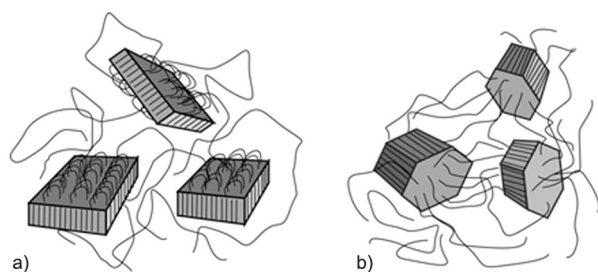
Figure 12. Sketch of supermolecular structures of α (a) and β (b) crystallites of iPP, which assumes that in the case of the β-phase, the connection between the amorphous and crystalline phases is through a high number of continuous prolonged-chains crystallites. The α crystallites consist of folded chains with few chains interconnecting lamellae. (adopted after Raab *et al.* [11]).

of connecting chains, as shown in Figure 12. Kotek *et al.* [7] mentioned how this structure can produce a long-range effect in the amorphous matrix and thus influence end-use properties. When recrystallizing this molecular structure, one can expect, the newly formed α crystallites will also comprise many interconnections. Together with mentioned thickening and improvement of lamellae, the number of tie chains between α crystallites should considerably affect the mechanical properties such as strength and stiffness, which are inherent qualities of α-phase.

The observed increase in the case of HD60, which is missing in the case of BE52 – *i.e.*, the material with double M_w than the HD60, can be explained by
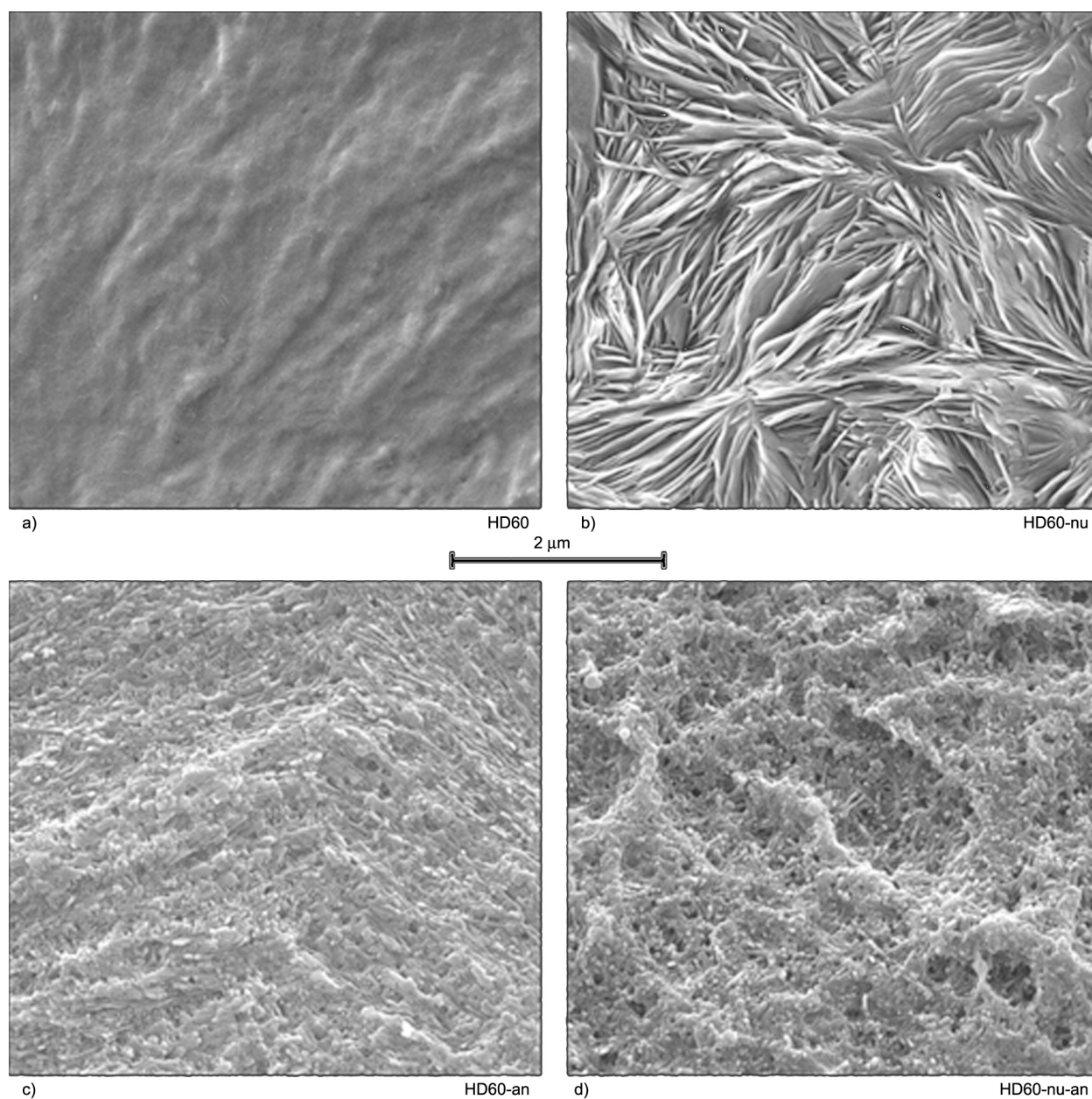

Figure 13. SEM micrographs of the etched surface of HD60 (a, c) and HD60-nu (b, d) before annealing (a, b) and after the treatment (c, d).

the tendency of very long chains to create entanglements. The entangled segments then rest primarily in the amorphous interlamellar space, not creating ties between lamellae, which should have a negligible long-range effect [11].

Figure 13 shows the microstructure of HD60-related materials. The untreated materials are in the top half showing a typical lamellar structure in the case of β-nucleated (Figures 13b and 13d) and not well-exposed lamellae of α-phase (Figures 13a and 13c). On the other hand, the bottom half shows the fine structure of α-phase lamellae, which is clear of an interlamellar amorphous mass. Since the time of chemical etching was the same, the better removal of the amorphous phase should be explained by changing the ratio of the rigid amorphous fraction to mobile amorphous fraction.

4. Conclusions

Annealing with a temperature above melting temperature of β-phase was confirmed as an effective way to perform the β- to α-phase transformation. It can lead to the improvement of supermolecular structure as thickening and enhancement of lamellae, and consequently mechanical behavior of the annealed polypropylene. According to the presented analysis, the significant increase in strength and stiffness, which was most evident in the case of the β- to α-transformed samples with lower molecular weight, should not be connected primarily with the perfection of the crystalline phase because it remained quite similar. Since the change in the mechanical behavior should be attributed to the different structure of the amorphous phase that comprises many interconnecting chains which pass through several lamellae, providing long-range effect and thus influencing end-use properties of polypropylene.

Acknowledgements

References

[1] Turner Jones A., Cobbold A. J.: The β crystalline form of isotactic polypropylene. Journal of Polymer Science. Part B: Polymer Letters, **6**, 539–546 (1968).
https://doi.org/10.1002/pol.1968.110060802

[2] Shinohara Y., Yamazoe K., Sakurai T., Kimata S., Maruyama T., Amemiya Y.: Effect of structural inhomogeneity on mechanical behavior of injection molded polypropylene investigated with microbeam X-ray scattering. Macromolecules, **45**, 1398–1407 (2012).
https://doi.org/10.1021/ma202178r

[3] Lotz B., Wittmann J. C., Lovinger A. J.: Structure and morphology of poly(propylenes): A molecular analysis. Polymer, **37**, 4979–4992 (1996).
https://doi.org/10.1016/0032-3861(96)00370-9

[4] Liu X., Miao X., Cai X., Shao J., Zou F., Song W., Qiao J., Wu C.: The orientation of the dispersed phase and crystals in an injection-molded impact polypropylene copolymer. Polymer Testing, **90**, 106658 (2020).
https://doi.org/10.1016/j.polymertesting.2020.106658

[5] Mi D., Zhou M., Zhang J.: Quantification of shish-kebab and β-crystal on the mechanical properties of polypropylene. Journal of Applied Polymer Science, **134**, 45052 (2017).
https://doi.org/10.1002/app.45052

[6] Brückner S., Meille S. V.: Polymorphism in crystalline polypropylene. in 'Polypropylene' (ed.: J. Karger-Kocsis) Springer, Dordrecht, 606–614 (1999).
https://doi.org/10.1007/978-94-011-4421-6_82

[7] Kotek J., Kelnar I., Baldrian J., Raab M.: Structural transformations of isotactic polypropylene induced by heating and UV light. European Polymer Journal, **40**, 2731–2738 (2004).
https://doi.org/10.1016/j.eurpolymj.2004.07.017

[8] Gahleitner M., Mileva D., Androsch R., Gloger D., Tranchida D., Sandholzer M., Doshev P.: Crystallinity-based product design: Utilizing the polymorphism of isotactic PP homo- and copolymers. International Polymer Processing, **31**, 618–627 (2016).
https://doi.org/10.3139/217.3242

[9] Wang J., Gahleitner M., Gloger D., Bernreitner K.: β-nucleation of isotactic polypropylene: Chain structure effects on the effectiveness of two different nucleating agents. Express Polymer Letters, **14**, 491–502 (2020).
https://doi.org/10.3144/expresspolymlett.2020.39

[10] Varga J.: Supermolecular structure of isotactic polypropylene. Journal of Materials Science, **27**, 2557–2579 (1992).
https://doi.org/10.1007/BF00540671

[11] Raab M., Kotek J., Baldrian J., Grellmann W.: Toughness profile in injection-molded polypropylene: The effect of the β-modification. Journal of Applied Polymer Science, **69**, 2255–2259 (1998).
https://doi.org/10.1002/(SICI)1097-4628(19980912)69:11<2255::AID-APP18>3.0.CO;2-Y

[12] Gajzlerova L., Navratilova J., Ryzi A., Slabenakova T., Cermak R.: Joint effects of long-chain branching and specific nucleation on morphology and thermal properties of polypropylene blends. Express Polymer Letters, **14**, 952–961 (2020).
https://doi.org/10.3144/expresspolymlett.2020.77

[13] Zhang D., Ding L., Yang F., Lan F., Cao Y., Xiang M.: Structural evolution of β-iPP with different supermolecular structures during the simultaneous biaxial stretching process. Polymer Journal, **53**, 331–344 (2021).
https://doi.org/10.1038/s41428-020-00430-6

[14] Čermák R., Obadal M., Poniížil P., Polášková M., Stoklasa K., Lengálová A.: Injection-moulded α- and β-polypropylenes: I. Structure vs. processing parameters. European Polymer Journal, **41**, 1838–1845 (2005).
https://doi.org/10.1016/j.eurpolymj.2005.02.020

[15] Čermák R., Obadal M., Poniížil P., Polášková M., Stoklasa K., Hečková J.: Injection-moulded α- and β-polypropylenes: II. Tensile properties vs. processing parameters. European Polymer Journal, **42**, 2185–2191 (2006).
https://doi.org/10.1016/j.eurpolymj.2006.03.014

[16] Glüge R., Altenbach H., Kolesov I., Mahmood N., Beiner M., Androsch R.: On the effective elastic properties of isotactic polypropylene. Polymer, **160**, 291–302 (2019).
https://doi.org/10.1016/j.polymer.2018.10.061

[17] Hedesiu C., Demco D. E., Kleppinger R., van den Poel G., Gijsbers W., Blümich B., Remerie K., Litvinov V. M.: Effect of temperature and annealing on the phase composition, molecular mobility, and the thickness of domains in isotactic polypropylene studied by proton solid-state NMR, SAXS, and DSC. Macromolecules, **40**, 3977–3989 (2007).
https://doi.org/10.1021/ma070014q

[18] van der Meer D. W., Milazzo D., Sanguineti A., Vancso G. J.: Oriented crystallization and mechanical properties of polypropylene nucleated on fibrillated polytetrafluoroethylene scaffolds. Polymer Engineering and Science, **45**, 458–468 (2005).
https://doi.org/10.1002/pen.20297

[19] Hou W-M., Liu G., Zhou J-J., Gao X., Li Y., Li L., Zheng S., Xin Z., Zhao L-Q.: The influence of crystal structures of nucleating agents on the crystallization behaviors of isotactic polypropylene. Colloid and Polymer Science, **285**, 11–17 (2006).
https://doi.org/10.1007/s00396-006-1475-x

[20] Ding L., Zhang D., Yan N., Zhang S., Wu T., Yang F., Lan F., Cao Y., Xiang M.: The structure changes of polypropylene precursor film with different die draw ratio during annealing. Polymer, **208**, 122958 (2020).
https://doi.org/10.1016/j.polymer.2020.122958

[21] Bai H., Luo F., Zhou T., Deng H., Wang K., Fu Q.: New insight on the annealing induced microstructural changes and their roles in the toughening of β-form polypropylene. Polymer, **52**, 2351–2360 (2011).
https://doi.org/10.1016/j.polymer.2011.03.017

[22] Shen J., Zhou Y., Lu Y., Wang B., Shen C., Chen J., Zhang B.: Later stage melting of isotactic polypropylene. Macromolecules, **53**, 2136–2144 (2020).
https://doi.org/10.1021/acs.macromol.9b01880

[23] Yang S., Yu H., Lei F., Li J., Guo S., Wu H., Shen J., Xiong Y., Chen R.: Formation mechanism and morphology of β-transcrystallinity of polypropylene induced by two-dimensional layered interface. Macromolecules, **48**, 3965–3973 (2015).
https://doi.org/10.1021/acs.macromol.5b00396

[24] Lotz B.: α and β phases of isotactic polypropylene: A case of growth kinetics 'phase reentrency' in polymer crystallization. Polymer, **39**, 4561–4567 (1998).
https://doi.org/10.1016/S0032-3861(97)10147-1

[25] Bai H., Deng H., Zhang Q., Wang K., Fu Q., Zhang Z., Men Y.: Effect of annealing on the microstructure and mechanical properties of polypropylene with oriented shish-kebab structure. Polymer International, **61**, 252–258 (2012).
https://doi.org/10.1002/pi.3180

[26] Bai H., Wang Y., Zhang Z., Han L., Li Y., Liu L., Zhou Z., Men Y.: Influence of annealing on microstructure and mechanical properties of isotactic polypropylene with β-phase nucleating agent. Macromolecules, **42**, 6647–6655 (2009).
https://doi.org/10.1021/ma9001269

[27] Na B., Li Z., Lv R., Zou S.: Annealing-induced structural rearrangement and its toughening effect in injection-molded isotactic polypropylene. Polymer Engineering and Science, **52**, 893–900 (2012).
https://doi.org/10.1002/pen.22156

[28] Chvátalová L., Navrátilová J., Čermák R., Raab M., Obadal M.: Joint effects of molecular structure and processing history on specific nucleation of isotactic polypropylene. Macromolecules, **42**, 7413–7417 (2009).
https://doi.org/10.1021/ma9005878

[29] Varga J., Mudra I., Ehrenstein G. W.: Highly active thermally stable β-nucleating agents for isotactic polypropylene. Journal of Applied Polymer Science, **74**, 2357–2368 (1999).
https://doi.org/10.1002/(SICI)1097-4628(19991205)74:10<2357::AID-APP3>3.0.CO;2-2

[30] Galeski A.: Crystallization. in 'Polypropylene' (ed.: Karger-Kocsis J.). Kluwer, Dordrecht, 135–141 (1999).
https://doi.org/10.1007/978-94-011-4421-6_19

[31] Brandrup J., Immergut E. H., Grulke E. A.: Polymer handbook. Wiley, New York (1999).

[32] Alexander L.: X-ray diffraction methods in polymer science. Wiley, New York (1970).

[33] Konishi T., Nishida K., Kanaya T.: Crystallization of isotactic polypropylene from prequenched mesomorphic phase. Macromolecules, **39**, 8035–8040 (2006).
https://doi.org/10.1021/ma060191b

[34] Koch T., Seidler S., Halwax E., Bernstorff S.: Microhardness of quenched and annealed isotactic polypropylene. Journal of Materials Science, **42**, 5318–5326 (2007).
https://doi.org/10.1007/s10853-006-0960-4

[35] Hermans P. H., Weidinger A.: On the determination of the crystalline fraction of polyethylenes from X-ray diffraction. Die Makromolekulare Chemie, **44**, 24–36 (1961).
https://doi.org/10.1002/macp.1961.020440103

[36] Turner Jones A., Aizlewood J. M., Beckett D. R.: Crystalline forms of isotactic polypropylene. Die Makromolekulare Chemie, **75**, 134–158 (1964).
https://doi.org/10.1002/macp.1964.020750113

[37] Uvarov V., Popov I.: Metrological characterization of X-ray diffraction methods for determination of crystallite size in nano-scale materials. Materials Characterization, **58**, 883–891 (2007).
https://doi.org/10.1016/j.matchar.2006.09.002

[38] Kotek J., Raab M., Baldrian J., Grellmann W.: The effect of specific β-nucleation on morphology and mechanical behavior of isotactic polypropylene. Journal of Applied Polymer Science, **85**, 1174–1184 (2002).
https://doi.org/10.1002/app.10701

[39] Yamamoto Y., Inoue Y., Onai T., Doshu C., Takahashi H., Uehara H.: Deconvolution analyses of differential scanning calorimetry profiles of β-crystallized polypropylenes with synchronized X-ray measurements. Macromolecules, **40**, 2745–2750 (2007).
https://doi.org/10.1021/ma062784s

[40] Beníček L., Chvátalová L., Obadal M., Čermák R., Verney V., Commereuc S.: Photodegradation of isotactic poly(1-butene): Multiscale characterization. Polymer Degradation and Stability, **96**, 1740–1744 (2011).
https://doi.org/10.1016/j.polymdegradstab.2011.08.001

[41] Chen Y-H., Mao Y-M., Li Z-M., Hsiao B. S.: Competitive growth of α- and β-crystals in β-nucleated isotactic polypropylene under shear flow. Macromolecules, **43**, 6760–6771 (2010).
https://doi.org/10.1021/ma101006e

[42] Varga J., Menyhárd A.: Effect of solubility and nucleating duality of *N,N′*-dicyclohexyl-2,6-naphthalenedicarboxamide on the supermolecular structure of isotactic polypropylene. Macromolecules, **40**, 2422–2431 (2007).
https://doi.org/10.1021/ma062815j